ELSEVIER

Biophysical Chemistry 86 (2000) 1–14

Biophysical Chemistry

www.elsevier.nl/locate/bpc

Molecular dynamics estimates of ion diffusion in model hydrophobic and KcsA potassium channels

Toby W. Allen[a,*], Serdar Kuyucak[b], Shin-Ho Chung[a]

[a] *Protein Dynamics Unit, Department of Chemistry, Australian National University, Canberra, ACT 0200, Australia*
[b] *Department of Theoretical Physics, Research School of Physical Sciences, Australian National University, Canberra, ACT 0200, Australia*

Received 28 December 1999; received in revised form 27 March 2000; accepted 29 March 2000

Abstract

Molecular dynamics simulations are carried out to obtain estimates of diffusion coefficients of biologically important Na^+, K^+, Ca^{2+} and Cl^- ions in hydrophobic cylindrical channels with varying radii and large reservoirs. Calculations for the cylindrical channels are compared to those for the KcsA potassium channel, for which the protein structure has recently been determined from X-ray diffraction experiments. Our results show that ion diffusion is maintained at reasonably high levels even within narrow channels, and does not support the very small diffusion coefficients used in some continuum models in order to fit experimental data. The present estimates of ion diffusion coefficients are useful in the calculation of channel conductance using the Poisson–Nernst–Planck theory, or Brownian dynamics. © 2000 Elsevier Science B.V. All rights reserved.

Keywords: Ionic diffusion coefficient; Molecular dynamics simulation; Ion channel; Conductance prediction; Poisson–Nernst–Planck

1. Introduction

The development of the patch-clamp technique has enabled the study of single channel currents across biological membranes, leading to an enormous amount of data on current–voltage (I–V) relationships in a large variety of ion channels, obtained under various conditions [1]. Due to a lack of detailed information on the structure of the proteins forming the membrane channels, interpretation of this wealth of data has so far relied on rather simple models, based on reaction rate or continuum theories [2]. These models serve a useful purpose in cataloging the available data, but because they have freely adjustable parameters, they are not very useful in relating the structure of the channels to their function (or vice versa), which is the ultimate goal of the

* Corresponding author. Tel.: +61-26-249-2931; fax: +61-26-247-2792.
E-mail address: toby.allen@anu.edu.au (T.W. Allen).

0301-4622/00/$ - see front matter
PII: S0301-4622(00)00153-8

channel models. The recent determination of the structure of the KcsA potassium [3] and the mechanosensitive MscL homolog [4] channels by X-ray diffraction has opened a new vista in channel studies by bringing this goal within reach. The preferred method for this purpose would be molecular dynamics (MD), where all the atoms in the channel system (protein + electrolyte) are simulated. Unfortunately, MD calculation of conductance is not computationally feasible as yet. We need roughly a 1000-fold increase in computer speed to reach the μs simulation regime that is necessary for the determination of conductance from MD simulations. In the mean time, one can attack the ion conductance problem by utilizing simpler models, provided the parameters used in these models can be determined from the more fundamental MD calculations.

The bottleneck in MD calculations is created by water molecules in the electrolyte. For a 150 mM NaCl solution, there are 370 water molecules for each Na^+ ion. Thus, in order to study conductance with a modest 20 Na^+ ions in the system, it would require the consideration of 22 200 extra atoms in MD simulations. This suggests that the first simplification would be to use the Brownian Dynamics (BD) method, where only the motion of ions is considered. In BD, water molecules in the system are integrated out, and their effect on ions is represented via random collisions, and friction and dielectric constants. A three-dimensional BD computer code that fully incorporates electrostatic potentials and forces from the solution of Poisson's equation has recently been developed and applied to various model ion channels [5–9]. These BD simulations have been quite successful in reproducing the observed properties of the ion channels considered. However, before these calculations can be accepted as relating structure to function, one needs to confirm that the parameters employed in BD, that is the diffusion coefficients of ions and the dielectric constants, are genuine features of the channel. Since an experimental determination of these quantities in ion channels is not possible, one can alternatively attempt to estimate them from computer experiments via MD simulations.

A further simplification of the ion conductance problem can be achieved by representing not only water, but also the ions in the system as a continuum. This so-called Poisson–Nernst–Planck (PNP) theory has been applied to a variety of ion channels, and numerous I–V curves have been fitted quite successfully using only a few parameters (see [10–15] for recent references, and the reviews [16,17] for earlier literature). To verify the applicability of the PNP theory to ion channels, one needs to resolve two issues. The first is to ensure that the parameters employed in the model are in the range predicted by MD calculations. The other is to check whether the mean field approximation holds in ion channels, which typically have radii smaller than the Debye length. The latter has recently been tested by comparing the predictions of PNP with those obtained from BD simulations [18,19]. These comparisons show that shielding effects are largely overestimated in PNP, leading to erroneous results for concentration profiles and ionic currents in narrow channels. Therefore PNP cannot describe the physics of ion channels. Nevertheless, the success of the PNP theory in fitting the channel data has been used in promoting its use in ion channels. To understand the origin of this success, despite the shortcomings of PNP as a physical model of ion channels, one needs to resolve the first issue, that is to inspect the parameters used in PNP calculations in the light of MD simulations.

The parameters in PNP essentially consist of the diffusion coefficient of ions, and the dielectric constants in the channel and the protein, as in BD. In most cases, the tertiary structure of the channels is not known and one has to include the channel dimensions and fixed charges as additional parameters. Once the molecular structure of a channel is determined, it can be implemented in PNP calculations to relieve it from these structural parameters, as has been recently done for the gramicidin A channel [15]. Even in the absence of structural knowledge at the molecular level, enough is known about channels to constrain these parameters to relatively small ranges. On the other hand, little is known about the dynamical parameters (especially diffusion coefficients), which are treated as completely free parameters in PNP, to be determined from fits to

the I–V data. Therefore, MD estimates of these parameters are essential in order to assess the reliability of the PNP results obtained so far. Here, we focus on ion diffusion coefficients rather than dielectric constants for the following reasons. First, the PNP results show very little sensitivity towards variations in dielectric constants [19], and therefore, the canonical values ($\varepsilon_{water} = 80$, $\varepsilon_{protein} = 2$) are often employed in PNP calculations. Even if these values were to be modified as a result of MD simulations, their effect on the final PNP results are too small to make any difference. In contrast, current is directly proportional to the diffusion coefficients of ions in the PNP theory, and thus, the results are very sensitive to their choice. In fact, the diffusion coefficient of a particular type of ion is the most important parameter in fitting the corresponding I–V curve. Unlike dielectric constants, diffusion coefficients obtained from PNP fits show large variations from their bulk values, ranging from an order of magnitude to several orders of magnitude reduction. One purpose of this study is to obtain MD estimates of ion diffusion coefficients in various channel models and demonstrate that such low levels of ion diffusion are, in fact, unrealistic.

Until recently, there has been little knowledge about the variation in ion diffusion coefficients with channel constitution and size, and little understanding of the mechanisms underlying these dependencies. This situation has changed with the appearance of several MD studies of ion diffusion, which include hydrophobic and hydrophilic cylindrical channels, with either periodic or closed boundaries [20,21], and model ion channels of β-barrel, α-helix bundles, leucine–serine peptide, alamethicin fungal peptide, and the nicotinic acetylcholine receptor [22,23]. Our purpose in this work was to present a more comprehensive and systematic survey of ion diffusion in channels. The effect of pore size and charge content on ion diffusion is studied employing simple hydrophobic channels with variable radius and of realistic length, with reservoirs. Such model channels have been employed in the majority of PNP calculations of ion conductance; hence the diffusion results obtained here provide a direct test for these PNP calculations. Besides the usual Na^+, K^+ and Cl^- ions, we also explore the diffusion of divalent Ca^{2+} ion, which plays an important role in some biological channels. In the second part of the paper, we study ion diffusion in the KcsA potassium channel, implementing its full molecular structure as determined from X-ray diffraction experiments [3]. Besides their intrinsic value, the KcsA results will also serve to check the robustness of the ion diffusion estimates obtained in the first part, using simple hydrophobic channels.

2. Model systems

2.1. Cylindrical channels

A generic channel model is most conveniently represented in MD simulations by cylindrical hydrophobic channels with fixed charges on them. These channels, illustrated in Fig. 1, are 25 Å in length, and have effective radii $R_{min} = 3$, 5 and 7 Å. Reservoirs, each of length 15 Å and radius 12 Å, are connected to the ends of the channel, which are large enough to provide a bulk-like environment for the ions. Corners joining the channel and reservoir borders are generated by a 5-Å radius circular arc, prior to the axial rotation to generate the pore. Periodic boundaries act at the $z = \pm 27.5$ Å planes.

In a previous study, we have shown that a hydrophobic wall lining need not be treated in atomic detail in MD simulations of narrow pores

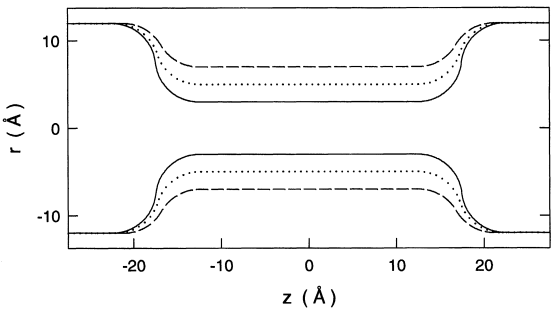

Fig. 1. Finite cylindrical channels with reservoirs. The three curves represent channels with radii 3, 5 and 7 Å. A three-dimensional channel model is generated by rotating the curves shown about the central axis by 180°.

[21]. Instead, one can employ a structureless one-dimensional potential function found by Boltzmann averaging the potential due to a cylindrical array of Lennard–Jones (LJ) 12–6 potential centers. Results have shown that there is very little impact on water structure, self and ion diffusion for this range of channel radii. A similar conclusion has been reached in a MD study of Na^+ ion diffusion in hydrophobic channels where the channel structure is explicitly included [22]. The potential function that best represents a cylindrical hydrophobic wall is found to be a LJ 5–3 potential of the form [21]:

$$V^{LJ}(\Delta) = \frac{3}{2}\varepsilon\left[\left(\frac{\sigma}{\Delta}\right)^5 - \frac{5}{3}\left(\frac{\sigma}{\Delta}\right)^3\right] \quad (1)$$

where $\Delta = a(z) - r$ is the radial distance from the point of infinite repulsion [at $r = a(z)$]. Assuming a van der Waals atomic radius of 1.4 Å, we place the point of infinite repulsion at $a(z) = R(z) +$ 1.4 Å. Eq. (1) is designed such that σ and ε correspond to the position and depth of the potential minimum, respectively. The parameters σ and ε are given the values 1.1 kT and 3.45 Å, respectively, which adequately represent the potential over the entire channel length and reservoirs [21].

An ion entering a narrow hydrophobic pore experiences an energy barrier associated with dehydration and image repulsion. Charged or polar amino acids in the channel protein usually provide a stabilizing potential such that the ion may be permitted to traverse the pore. In one series of simulations, we mimic this effect by placing a ring of eight oxygen-like atoms, each with the charge $-e/8$, at $z = 0$ Å, 1.4 Å behind the effective pore radius. Charges with similar strength have been employed in PNP studies of cylindrical channels [10,14].

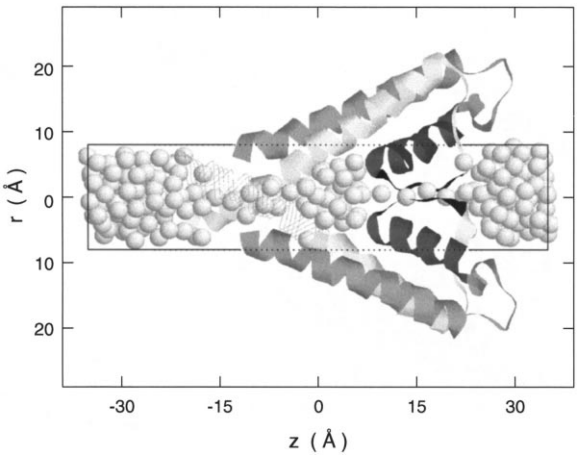

Fig. 2. Hydrated potassium channel structure after 150 ps of dynamics. The outer helices and turrets (light gray ribbons), pore helices (dark gray ribbons), selectivity filter (narrow black ribbons), and inner helices (white ribbons) for two subunits of the tetramer are drawn. The intracellular half of one inner helix has been replaced by thin strands to reveal the water positions within the long hydrophobic pore region.

2.2. The KcsA potassium channel

Fig. 2 shows two of the four subunits of the tetramer of peptide chains which form the KcsA potassium channel protein structure. The initial coordinates for all 388 experimentally determined amino acid residues have been taken from the Protein Data Bank set *1bl8*, described by Doyle et al. [3]. The amino acid sequence is divided into segments of interest in Table 1. The van der

Table 1
KcsA signature amino acid sequence[a]

Segment	Residues	
N-terminal	22	$-CH_3-CO$
Outer helix	23–61	ALHWRAAGAATVLLVIVLLAGSYLAVLAERGAPGAQLIT
Pore helix	62–74	YPRALWWSVETAT
Selectivity filter	75–79	TVGYG
Inner helix	80–119	DLYPVTLWGRCVVVAVVVMVAGITSFGLVTAALATWFVGREQ
C-terminal	120	$-CH_3-NH$

[a]The residues within each subunit of the experimentally determined potassium channel protein structure are divided into segments.

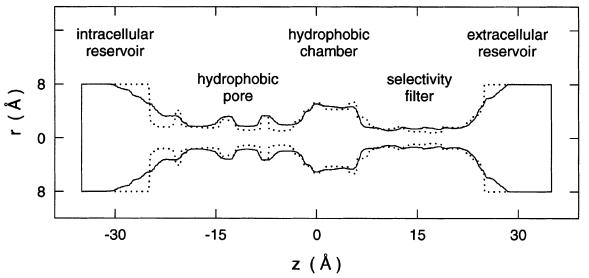

Fig. 3. The initial (dotted curve) and time averaged (solid curve) pore radii (accounting for van der Waals radii) are shown. Indicated are the selectivity filter, hydrophobic chamber, hydrophobic pore and the intracellular and extracellular reservoirs.

Waals corrected channel radius profile for the initial protein coordinates, in the absence of any water, is shown in Fig. 3 as a dotted curve. The channel extends from $z \approx -25$ to 25 Å. The selectivity filter region adjacent to the extracellular space extends from $z \approx 8$ to 22 Å, with a mean radius of ~ 1.4 Å for the empty channel. This region is hydrophilic in nature, being lined with carbonyl and hydroxyl oxygen atoms. There is a large hydrophobic chamber region on the intracellular side of the selectivity filter with an average radius of 6 Å extending from $z \approx -2$ to 8 Å. A strong stabilizing potential is provided by the pore helices, which are directed at the center of this region. The long thin hydrophobic chamber formed by the inner helices leading to the intracellular space extends from $z \approx -20$ to -2 Å, with a minimum radius of ~ 1.5 Å. Reservoirs ($25 < |z| < 35$ Å) are formed by a bounding cylinder of radius 8 Å. A harmonic potential, with a force constant of 100 kT/Å^2, acts only on water oxygen atoms and ions outside this cylinder.

A survey of constraints emulating interactions with a lipid bilayer has been carried out for these simulations. The shape of the protein in the selectivity filter and hydrophobic chamber regions are found to be relatively insensitive to constraints applied to the inner and outer helices. In a related article [24], we demonstrate that these constraints have little bearing on channel function, and in particular ion discrimination. We apply 20 kT/Å^2 force constants to all inner and outer helix α carbons. Similar strength restraining potentials have been used in model acetylcholine receptor studies [22]. Gating studies of the KcsA potassium channel have indicated that the crystallographic structure, with a narrow hydrophobic pore, may in fact correspond to a closed state in which conduction does not take place [25]. Therefore, in separate simulations with ions in this long narrow region, we reduce the constraints on the α carbons of the outer helix and the extracellular half of the inner helix (residues 80–99) to 10 kT/Å^2 and those on the intracellular half of the inner helix (residues 100–119) to just 1 kT/Å^2, thus permitting this region to expand in the presence of a hydrated ion.

3. Simulations

MD simulations are performed using the CHARMM v. 25 code [26] with the CHARMM19 united atom parameter set. By comparing electrostatic profiles with neutral and charged side-chains on acidic residues [24], it was determined that most acidic and basic groups are likely to be neutral in order to make this channel conduct. Neutral residues for arginine, aspartic acid and glutamic acid [27] are used with the CHARMM19 set. We employ the SPC/E water model [28] for all simulations, because of its ability to accurately reproduce bulk water and ion properties. When the TIP3P water model [29], and its flexible version [30] are used, water molecules fail to solvate the hydrophilic interior of the selectivity filter. This would lead to an artificial ion solvation environment and erroneous ion diffusion values. The ion–water parameters of Pettit and Rossky [31], as tested with SPC/E [32], are employed. Potential parameters for the Ca^{2+} ion are taken from Lynden–Bell and Rasaiah [20]. Ion–ion LJ parameters are taken from Heinzinger [33], and ion–protein interactions are determined with the use of standard combination rules.

A time step of 1 fs is used in the simulations with the Verlet MD algorithm. Velocity rescaling at 1-ps intervals leads to temperatures of 298 ± 1 K. Coordinates are saved every 0.1 ps for trajectory analysis. Periodic boundaries are enforced with a single image placed at each end of

the channel in the axial direction. The treatment of long-range forces can influence self and ion diffusion [34,35]. A noticeable reduction in both self and ion diffusion in bulk simulations is observed when the long-range cut-off is reduced from 12 to 8 Å [34]. Therefore, a minimum truncation distance of 12 Å is maintained in the present simulations. A switched force cut-off for electrostatic interactions and a switched potential cut-off for LJ 12–6 interactions are applied to atoms at 12 Å, slowly turned off from 8 Å [26]. Non-bonded interaction lists are recorded up to 13 Å and are updated at 5–10-fs intervals.

The water in the cylindrical channels is sampled from pre-equilibrated bulk SPC/E coordinates, using the procedure outlined in Allen et al. [21]. The number of water molecules inside the 3-, 5- and 7-Å channels is 336, 409 and 513, respectively, leading to average densities of 1.000 $\pm$ 0.001 g/cm^3. An initial molding of the system, involving a slow turn-on of the wall potential [21], is performed. Prior to the introduction of ions into the channel, equilibration of the water-filled system consists of 100 steepest descent minimization steps, 50 ps of equilibration, and 100 ps of dynamics for analysis. A single Na^+, K^+, Ca^{2+} or Cl^- ion is then included, without removing any water molecules. Not removing water molecules when introducing an ion has a negligible effect on mean water density in the system. After a further 100 minimization steps and 50 ps of equilibration, 0.5–1 ns of dynamics is carried out for each ion in each system. When an ion leaves the channel region it is replaced at the center, and the simulation is restarted.

The sampling procedure for the potassium channel simulation is more involved owing to the complex shape of the protein. The water in the reservoirs is handled separately by sampling from the equilibrated bulk water in the range $|z| > 25$ Å with radius less than 8 Å. The water within the channel ($|z| \leq 25$ Å) is taken from 150-ps simulations with a simplified model of the potassium channel [36]. This simplified model employs a LJ 5–3 pore lining throughout, except for the narrow hydrophilic selectivity filter region where protein is treated explicitly. Water coordinates inside and outside the channel are then combined, and any water molecule with an oxygen atom center closer than 2 Å to a protein atom center is moved away or into a reservoir. The number of water molecules remaining after this procedure is 210. Equilibration with the entire protein for 150 ps is carried out prior to the addition of ions.

Three K^+ ions are added to the potassium channel at various positions, creating multiple ion configurations similar to those anticipated by experimental data [3] and simple model simulations [36]. In each simulation one ion always resides in the wide hydrophobic chamber region ($-2 \leq z \leq 8$ Å). A total of 3.6 ns of simulation is carried out in 17 separate tests in the absence of any external field. In a separate set of simulations, a single K^+ ion is placed at one of several positions in the long hydrophobic pore region, and a series of 16×200-ps simulations are carried out in order to compute the average diffusion coefficients in this narrow region. For a comparison, several simulations, each of 200 ps in length, are carried out with a single Na^+ or Cl^- ion at various positions within the hydrophobic chamber and long pore regions of the potassium channel. Due to the large size of the Cl^- ion (Pauling radius $\sim$1.8 Å), and the small size of the long pore, dynamics simulations are not successful with this ion in the region $-20 \leq z \leq -2$ Å.

Water self-diffusion and ion diffusion coefficients are calculated by averaging the mean square fluctuations of the oxygen and ion position vectors. Statistical uncertainty is minimized by using an overlapped data procedure [37], where a window of 0.5–10 ps is slid through the sample data. Here windows of 0.5 ps or less are ignored as they correspond to the inertial motion within the hydration cage. Before calculating diffusion coefficients, the center of mass of the system is subtracted to remove any net momentum associated with the periodic boundary. We consider only axial diffusion given by the formula:

$$D_z = \frac{1}{2}\frac{\mathrm{d}}{\mathrm{d}t}\langle [z(t) - z(0)]^2 \rangle \qquad (2)$$

At the completion of pure water simulations,

100 ps of production is divided into five samples of 20 ps each, from which a self-diffusion coefficient is calculated. Ion diffusion coefficients involve breaking MD production into several 100–300-ps samples.

4. Results and discussion

4.1. Cylindrical channels

We begin with a summary of channel water properties, since the structure and dynamics of channel water is likely to have some influence on ion mobility. We observe that within the finite length of the cylindrical channels, the water radial density profiles are very similar to those seen within periodic cylinders [21,30]. Water molecules are ordered in cylindrical shells and may exhibit some degree of layering in the axial direction. Previous results [21] have shown that only a moderate degree of ordering is observed in hydrophobic channels with effective radii of 3, 5 and 7 Å, and thus self-diffusion levels are not expected to be greatly attenuated. The hydrophobic nature of the pore lining leads to an exclusion zone of approximately 0.7–0.8 Å, with the first peak in the radial density profile sitting at approximately 1.2 Å from the effective pore lining. Inspection of the average water densities in Table 2 shows that the 5 and 7-Å channels maintain near bulk density, but the density in the 3-Å channel is reduced to 80% of bulk. This reduction in the narrow channel is presumably due to the overestimation of the repulsive wall potential, which has been determined from the potential of an atomic wall at water density. It is possible that the actual density of atoms forming the protein wall is lower than that of water. In the presence of a ring of partial charges, the density is raised to 87% of bulk in the 3-Å channel and to 98% of bulk in the larger ones.

Also listed in Table 2 are axial self-diffusion estimates and their percentages with respect to the bulk estimates given in Table 3. Self-diffusion coefficients are seen to be of the same order as the bulk value. The higher level of self-diffusion in the narrow 3-Å channel can be associated with decreased water density. For example, in a periodic cylinder of radius 3.1 Å, where the bulk density is maintained [21], self-diffusion drops to $\sim 2/3$ of the bulk value. The presence of a ring of charges diminishes self-diffusion by roughly half in each channel size. The larger drop in the narrow channel is again associated with the increase in density. We note that the mean values of water self-diffusion within the range $|z| \leq 12.5$ Å (i.e. inside the channel), and the smaller range $|z| \leq 5$ Å, are indistinguishable to within the uncertainties of each measurement.

Table 2
Pure water self-diffusion coefficients within cylindrical channels[a]

R_{min} (Å)	ρ (g/cm^3)	D_z (Å/ps)	% Bulk
No charges			
3	0.50	0.26 ± 0.02	$112 \pm 12\%$
5	0.96	0.17 ± 0.02	$74 \pm 11\%$
7	0.95	0.20 ± 0.02	$86 \pm 11\%$
With charges			
3	0.87	0.10 ± 0.02	$39 \pm 10\%$
5	0.98	0.09 ± 0.02	$39 \pm 10\%$
7	0.98	0.09 ± 0.02	$39 \pm 10\%$

[a] Estimates of axial self-diffusion are given for channel radius $R_{min} = 3$, 5 and 7 Å, with and without a ring of negative partial charges. Only water molecules within the range $-12.5 \leq z \leq 12.5$ Å are included in diffusion calculations. Errors are one standard error of means.

Table 3
Bulk reference values for water and ions: bulk properties r_{max}, r_{min}, n, and D are the first minima and maxima in the RDF, the first hydration number and the diffusion coefficient respectively[a]

Property	Water	Na^+	K^+	Ca^{2+}	Cl^-
r_{max} (Å)	2.76 ± 0.04	2.32 ± 0.04	2.76 ± 0.04	3.32 ± 0.04	
r_{min} (Å)	3.36 ± 0.04	3.10 ± 0.08	3.65 ± 0.15	3.2 ± 0.2	3.92 ± 0.14
n	4.10 ± 0.06	5.56 ± 0.03	7.2 ± 0.4	7.90 ± 0.02	7.9 ± 0.4
D (Å^2/ps)	0.23 ± 0.01	0.09 ± 0.01	0.14 ± 0.01	0.053 ± 0.006	0.13 ± 0.03
Experiment					
r_{max} (Å)	2.84 [39]	2.4 [40]	2.7 [41]	2.46 [42]	3.2 [43]
n	4.4 [39]	4–6 [40]	5–6 [41]	10.0 [42]	5.5 [43]
D (Å^2/ps) [38]	0.23	0.133	0.196	0.079	0.203

[a]Simulations are performed with 528 SPC/E water molecules in a periodic box of side 25.08 Å at temperature 298 K. After 50 ps of heating and equilibration, 100 ps of MD is used to determine the self-diffusion coefficient. A single Na^+, K^+, Ca^{2+} or Cl^- ion is added, leaving 525 SPC/E molecules. After 100 steps of steepest descent minimization and 50 ps of equilibration, 500 ps of trajectory data is used to produce the ion diffusion estimates. References for experimental results are quoted in the table.

Table 4
Ion diffusion results within cylindrical channels[a]

Ion	R_{min} (Å)	n	D_z (Å^2/ps)	% Bulk
No charges				
Na^+	3	4.96 ± 0.01	0.11 ± 0.01	$122 \pm 25\%$
	5	5.39 ± 0.03	0.11 ± 0.03	$122 \pm 47\%$
	7	5.88 ± 0.05	0.07 ± 0.01	$78 \pm 20\%$
K^+	3	4.83 ± 0.08	0.13 ± 0.04	$93 \pm 35\%$
	5	8.5 ± 1.2	0.11 ± 0.02	$79 \pm 20\%$
	7	7.9 ± 0.5	0.10 ± 0.01	$71 \pm 12\%$
Ca^{2+}	3	7.36 ± 0.02	0.18 ± 0.06	$340 \pm 150\%$
	5	7.96 ± 0.02	0.027 ± 0.004	$51 \pm 13\%$
	7	7.96 ± 0.01	0.028 ± 0.004	$53 \pm 14\%$
Cl^-	3	5.80 ± 0.03	0.14 ± 0.04	$108 \pm 55\%$
	5	8.1 ± 0.4	0.07 ± 0.04	$54 \pm 43\%$
	7	9.0 ± 1.0	0.12 ± 0.02	$92 \pm 37\%$
With charges				
Na^+	3	5.21 ± 0.02	0.040 ± 0.009	$12 \pm 7\%$
	5	5.82 ± 0.12	0.048 ± 0.009	$53 \pm 16\%$
	7	5.85 ± 0.08	0.048 ± 0.008	$53 \pm 15\%$
K^+	3	4.06 ± 0.08	0.017 ± 0.009	$12 \pm 7\%$
	5	8.5 ± 0.8	0.008 ± 0.02	$56 \pm 21\%$
	7	8.1 ± 0.6	0.11 ± 0.02	$81 \pm 18\%$
Ca^{2+}	3	7.00 ± 0.01	0.0092 ± 0.0006	$17 \pm 3\%$
	5	7.99 ± 0.01	0.019 ± 0.01	$36 \pm 10\%$
	7	8.02 ± 0.01	0.028 ± 0.02	$53 \pm 12\%$
Cl^-	3	5.3 ± 0.3	0.82 ± 0.32	$631 \pm 392\%$
	5	$7.7 \pm .07$	0.12 ± 0.02	$85 \pm 22\%$
	7	8.4 ± 1.5	0.22 ± 0.03	$169 \pm 62\%$

[a]Estimates of axial ion diffusion are given for $R_{min} = 3$, 5 and 7 Å (with ion in the range $-12.5 \le z \le 12.5$ Å), with and without charge rings. Errors are one standard error of means. Also listed are the first hydration numbers of the ions (n) calculated from radial distribution functions.

This indicates that the ring of charge is polarizing all of the water in the pore to a similar extent, and that this increased ordering of molecules is not restricted to the vicinity of the ring.

The hydration waters of an ion can, to some degree, determine the ability of an ion to diffuse within channel environments. Except for special situations where a bare ion may diffuse through well organized zones of water molecules and remain hydrated (as suggested by Allen et al. [21], the ion will generally translate with its first hydration shell intact. This is a consequence of the long residence times of first-shell hydration water molecules (e.g. Na^+ has a residence time of $\sim$10–40 ps [32,44]). In general, the more coordinating molecules an ion has, the greater the resistance to its diffusion. We have calculated radial distribution functions for each ion in each channel to see if the pore size has any effect on them. The bounds of the first hydration shell of each ion type are fairly independent of the channel situation, with the positions of the first maximum and minimum residing near their bulk values, quoted in Table 3. The first hydration number, however, varies depending on the pore size and the local water density. A list of first hydration numbers within cylindrical channel segments is given in Table 4, which can be compared to the bulk values provided in Table 3.

Because the first minima in the bulk radial distribution functions of Na^+, K^+ Ca^{2+} and Cl^- ions reside at approximately 3.1, 3.65, 3.2 and 3.92 Å, respectively, the first hydration shells are not expected to fit inside spheres of radii less than 4.5, 5.05, 4.6 and 5.32 Å, respectively. Naively, one could predict that the 3-Å cylindrical pore would reduce the first hydration number of all four ions, the 5-Å pore would reduce the first hydration number of K^+ and Cl^- ions slightly, while Na^+ and Ca^{2+} would remain unaltered, and that the 7-Å channel would have little effect on the first hydration shells of any of these ions. However, because the intrapore water is not bulk-like, this simple geometrical argument does not apply so straightforwardly. In reality, the pore water forms well organized shells of high density. If the ion resides near a band of high density water, then it could have a large number of coordinating molecules in a reduced volume. In the 3-Å channel, reduced coordination numbers were observed for all ions. The Na^+, K^+, Ca^{2+} and Cl^- ions suffered hydration losses of 0.6, 2.4, 0.5 and 2.1 respectively. One would expect the axial diffusion of ions to be enhanced by these reduced hydration numbers. In the 5-Å channel, all ions have roughly maintained bulk coordination. Only the Na^+ ion remains slightly dehydrated (n is 0.3 smaller than bulk), which is presumably due to the close packing of the Na^+ solvation shell, such that it is unable to make full use of the neighboring shells of high density water. In contrast, Ca^{2+} and the larger K^+ and Cl^- ions exceed the bulk quotas. Within the largest 7-Å channel, all ions experience greater than bulk solvation. In each channel, the ions tend to reside in regions of low water density, solvated by the bands of high density water, as illustrated by Allen et al. [21]. The inclusion of a charged ring leads to a small decrease in the hydration numbers as they provide a competing source of polarization to the ion. The Na^+ ion, with a slightly increased solvation, proves to be an exception, possibly as a result of its compact coordination shell.

Table 4 lists the ion diffusion results within our model hydrophobic channels. Ion diffusion inside the cylindrical segments of the model channels remains of the same order as the bulk for all pore sizes and for all ion types. All monovalent ions have near bulk diffusion values in the narrow 3-Å channel, while that of the Ca^{2+} ion is particularly enhanced. This behavior can be understood in terms of the potential barrier associated with solvation losses and image repulsion that leads to a large force on ions, especially on the divalent Ca^{2+} ion. It can be noted that the Na^+ diffusion value in a 3.1-Å radius periodic cylinder, which does not possess an energy gradient due to image repulsion, is only $\sim$25% of the bulk [21]. Thus, while increased water mobility does contribute to the enhancement of ion diffusion, the majority of the effect comes from image repulsion. Finally, as predicted, there is a strong correlation between the diffusion coefficient and the hydration number. Ions tend to have greater diffusion in the narrow channel where they are not fully solvated and where mean water density is low.

The presence of a charge ring in the channel leads to the cancellation of the potential barrier for cations, and as a result, there is a substantial decrease in cation diffusion (Table 4). The effect of the external charges on ion diffusion is largest for the narrow channel, where the image repulsion barrier is highest and decreases with increasing radius. Since a channel is unlikely to conduct without charges, the estimates in this case provide more realistic values for ion diffusion. The lowest diffusion is observed for the K^+ ion in the narrow 3-Å channel at 12% of bulk, which quickly increases to near bulk values in larger channels. In the case of the Cl^- ion, the combined influences of hydration losses and repulsive external potential quickly expels the ion from the pore, leading to larger diffusion coefficients compared to the case without charges. The effect of these external charges is again largest in the 3-Å channel. The Cl^- ion is always ejected from the channel within 30 ps after the 50-ps equilibration period.

Since the ion diffusion results provided in Table 4 are average values over the entire channel length ($|z| \leq 12.5$ Å), they may be directly compared to the mean coefficients employed in PNP calculations. We find no evidence of greatly reduced ion diffusion in any of the channels, with or without fixed charges, that would justify the values used in PNP calculations. The PNP fits to the calcium channel [13] provide an extreme example: the Ca^{2+} and Na^+ diffusion coefficients have been reduced by 5000-fold and 400-fold, respectively, from their bulk values in order to fit the data. Our results in Table 4 suggest a maximum of an order of magnitude reduction for either ion under similar conditions. Another anomaly in the applications of PNP appears in the relative magnitude of the cation and anion diffusion employed, the latter being reduced by an order of magnitude compared to the former, in order to suppress the anion current across the channel [10]. The results in Table 4 for neutral and cation selective channels (lined with negative charges) suggest that anion diffusion coefficients will not experience such attenuation. Although anions will be excluded from the negatively charged pore by the repulsive electrostatic force, once inside, they will experience translational freedom similar to that of cations.

4.2. The potassium channel

We compare the above findings for the cylindrical channels to those for the known KcsA potassium channel. The structure of the potassium channel protein and water after 150 ps of simulation is shown in Fig. 2. It is clear from this figure that the water is solvating the entire pore of this channel, including the narrow hydrophobic region towards the intracellular space. Fig. 3 displays the time averaged minimum effective pore radius calculated from the last 100 ps of dynamics as a solid curve. The pore is still quite narrow after hydration, especially in the segment $-20 \leq z \leq -15$ Å, and it offers small pockets of wider pore for an ion to reside. Thus, we anticipate some difficulty for ions to translate in parts of this pore. There is evidence that the structure determined by Doyle et al. [3] may correspond to a closed state of the KcsA channel [25]. Nevertheless, diffusion estimates in the pore currently being studied will provide interesting comparisons with our model channels. We note that oxygen atoms (usually associated with polar or charged groups) reside away from the pore lining by at least 1 Å in the region $-25 \leq z \leq 8$ Å, and thus this segment appears to have maintained its hydrophobic nature after equilibration with water. Table 5 includes self-diffusion estimates for the pure water-filled potassium channel, broken into three segments: the selectivity filter ($8 < z \leq 22$ Å); the hydrophobic chamber ($-2 < z \leq 8$ Å); and the long hydrophobic pore ($-20 < z \leq -2$ Å). Only those waters within the channel pore are included in the density and diffusion estimates. If a water oxygen resides within the time averaged minimum pore radius at that axial position (z), then it is included in the sums. This excludes molecules embedded in the protein outside the pore. Throughout the entire channel and the reservoirs, the water density remains roughly the same as the bulk. Despite the small dimensions of the long hydrophobic pore, and the hydrophilic nature of the selectivity filter region, self-diffusion remains above 1/4 of bulk self-diffusion throughout the

Table 5
Pure water self-diffusion coefficients within the potassium channel[a]

Segment	ρ (g/cm^3)	D_z (Å^2/ps)	% Bulk
$8 \le z \le 22$ Å	1.06	0.06 ± 0.05	$26 \pm 21\%$
$-2 \le z \le 8$ Å	1.01	0.09 ± 0.01	$39 \pm 6\%$
$-20 \le z \le -2$ Å	1.01	0.06 ± 0.01	$26 \pm 5\%$

[a] Errors are one standard error of means.

channel. This is an indication that ion diffusion may not be greatly attenuated within the potassium channel.

A list of first hydration numbers within hydrophobic regions of the potassium channel is given in Table 6. Inside the hydrophobic regions of the potassium channel, the K^+ ion experiences less than bulk first shell coordination throughout. In the hydrophobic chamber the ion has approximately 0.7 less water than in the bulk, whereas in the long narrow pore the ion can lose as many as 2.6 hydration waters due to the small dimensions of the pore. Despite these solvation losses, the K^+ ion is not seen to experience a potential energy barrier [24]. We expect large ion mobility in this region due to the reduced solvation environment and absence of polar groups to restrict ion movement. The chloride ion, on the other hand, has exceeded its bulk quota of hydration waters in the chamber region, possibly in an attempt to shield the repulsive electrostatic interaction with the pore helices and selectivity filter. A Na^+ ion is seen to remain nearly fully solvated throughout the entire wide chamber and long hydrophobic pore regions.

Ion coordination inside the selectivity filter region is more complex than in the hydrophobic segments of the potassium channel due to the interplay with polar carbonyl and hydroxyl oxygens. The ability of this region to cause ion discrimination has been studied in simplified [36], and complete [24] potassium channel models. Brownian dynamics simulations suggest that two K^+ ions reside in equilibrium positions in the selectivity filter-chamber region until a third ion enters the channel; then one of the resident ions is quickly ejected from the channel [8]. An estimation of ion diffusion in such a situation is not very meaningful. Furthermore, this is a narrow hydrophilic region that cannot be directly compared to our simple model channels. Therefore, the selectivity filter region is not analyzed any further in the present study.

We list in Table 6 ion diffusion results within the potassium channel. Again we observe no evidence of greatly attenuated anion diffusion inside the wide hydrophobic chamber, with 38% of bulk diffusion on average. In this region the K^+ ion exhibits approximately half of the bulk diffusion, which is roughly in agreement with the value for the 5-Å model cylindrical channel. In the long hydrophobic pore, the diffusion of the K^+ ion varies depending on the position of the ion. When an ion is placed near the wider pocket at $z = -15$ Å, little ion translation is observed, whereas an ion placed near $z = -10$ Å will move quickly towards the wide chamber region. Fig. 4 shows the range of mean square displacement curves from which diffusion coefficients are

Table 6
Ion diffusion within the potassium channel[a]

Ion	Segment (Å)	n	Dz (Å^2/ps)	% Bulk
Na^+	$-2 \le z \le 8$ Å	5.93 ± 0.02	0.015 ± 0.002	$17 \pm 4\%$
	$-20 \le z \le -2$ Å	5.4–5.7	0.03 ± 0.01	$37 \pm 16\%$
K^+	$-2 \le z \le 8$ Å	3.54 ± 0.09	0.07 ± 0.008	$50 \pm 9\%$
	$-20 \le z \le -2$ Å	4.6–6.2	0.12 ± 0.07	$86 \pm 56\%$
Cl^-	$2 \le z \le 8$ Å	9.0 ± 0.4	0.05 ± 0.02	$38 \pm 24\%$
	$-20 \le z \le -2$ Å	–	–	–

[a] Errors are one standard error of means. Also listed are the first hydration numbers of the ions (n) calculated from radial distribution functions for water oxygen atoms only.

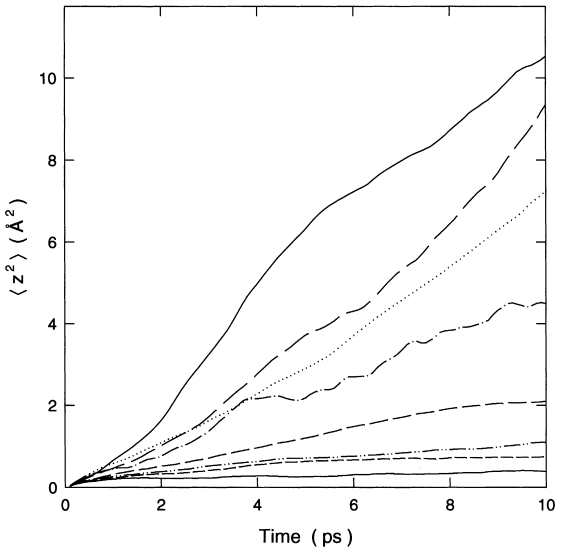

Fig. 4. K^+ ion diffusion in the potassium channel. The K^+ ion mean square displacements within the long hydrophobic pore region ($-20 \le z \le -2$ Å) of the potassium channel for selected 100 ps samples are shown.

determined. It can be seen that within the long pore, the diffusion ranges from near zero up to almost four times the bulk value. The average value of K^+ diffusion inside this region is 86% of the bulk. The fast motion of ions in this region is in agreement with trajectories observed in Brownian dynamics simulations [8]. While the Na^+ ion shows approximately 1/3 of bulk ion diffusion on average throughout the narrow long pore region, its coefficient is reduced in the wide chamber to just 1/6 of the bulk. Whereas multiple K^+ ion configurations in the selectivity filter and chamber could be created to eliminate deep energy wells [24], this is not possible for Na^+ because of the discriminatory property of the selectivity filter. As a result, the single Na^+ ion in the chamber used for this diffusion estimate is very stable and lacks translational freedom.

Ion diffusion results within the model channels and the potassium channel may be compared to other biological channels. Within channels of dimensions smaller than 3 Å, diffusion processes are complicated by ion–protein interactions. The creation of local minima in the energy profiles of such pores leads to permeation mechanisms, which are dependent on the channel type, and may be controlled by ion–ion interactions as well as diffusive processes. Thus, it is difficult to make comparisons between channels for narrow pores, such as the long hydrophobic pore of the potassium channel (radius ~ 2 Å); leucine–serine peptide and helix bundles of alanine residues with radii of 2–3.5 Å [22,23]; and gramicidin [45] with a radius of ~ 2 Å. However, comparisons can be made with wider pores, which tend to have hydrophobic linings and only shallow energy minima. The M2 helix bundle with the narrowest radius, 6 Å, supports approximately 60–70% of the bulk Na^+, K^+ and Cl^- ion diffusion on average; while the alamethicin fungal peptide, with a radius between 3.0 and 5.2 Å supports 40–50% of the bulk diffusion for all three ion types [22,23]. These results compliment the diffusion coefficients for all three monovalent ions in our 3–7-Å hydrophobic channels, and to the K^+ ion coefficient in the hydrophobic chamber of the potassium channel.

5. Conclusions

In this article, we have performed MD simulations to investigate the influence of pore size and charge content on the diffusion of different ion species commonly found in biological ion channels. We have employed simple channel models of realistic length and radii, and made comparisons with the KcsA potassium channel, for which an experimental structure has recently been determined. All ion types maintained reasonably high levels of diffusion within hydrophobic channels of radius 3–7 Å, with or without the action of external charges, as well as in the hydrophobic segments of the potassium channel. Our estimates of ion diffusion demonstrate that ion mobility does vary from the bulk value according to the channel size and charge content, but this variation is never of several orders of magnitude, as employed in some PNP fits to current–voltage data. We hope that in future phenomenological studies of ion permeation, the systematic ion diffusion results presented here will provide a useful

guide so that they will not be treated as free parameters that may be arbitrarily lowered to match experimental findings.

Acknowledgements

This work was supported by grants from the Australian Research Council and the National Health and Medical Research Council of Australia. The calculations upon which this work is based were carried out with the Alpha Cluster and Silicon Graphics Power Challenge of the ANU Supercomputer Facility.

References

[1] B. Hille, Ionic Channels of Excitable Membranes, 2nd ed., Sinauer Associates Inc, Sunderland, Massachusetts, 1992.
[2] D.G. Levitt, Interpretation of biological ion channel flux data — reaction-rate versus continuum theory, Annu. Rev. Biophys. Biophys. Chem. 15 (1986) 29–57.
[3] D.A. Doyle, J.M. Cabral, R.A. Pfuetzner, A. Kuo, J.M. Gulbis, S.L. Cohen, B.T. Chait, R. MacKinnon, The structure of the potassium channel: molecular basis of K^+ conduction and selectivity, Science 280 (1998) 69–77.
[4] G. Chang, R.H. Spencer, A.T. Lee, M.T. Barclay, D.C. Rees, Structure of the MscL homolog from Mycobacterium tuberculosis: a gated mechanosensitive ion channel, Science 282 (1998) 2220–2226.
[5] S.C. Li, M. Hoyles, S. Kuyucak, S.H. Chung, Brownian dynamics study of ion transport in the vestibule of membrane channels, Biophys. J. 74 (1998) 37–47.
[6] M. Hoyles, S. Kuyucak, S.H. Chung, Computer simulation of ion conductance in membrane channels, Phys. Rev. E58 (1998) 3654–3661.
[7] S.H. Chung, M. Hoyles, T.W. Allen, S. Kuyucak, Study of ionic currents across a model membrane channel using Brownian dynamics, Biophys. J. 75 (1998) 793–809.
[8] S.H. Chung, T.W. Allen, M. Hoyles, S. Kuyucak, Permeation of ions across the potassium channel: Brownian dynamics studies, Biophys. J. 77 (1999) 2517–2533.
[9] T.W. Allen, M. Hoyles, S. Kuyucak, S.H. Chung, Molecular and Brownian dynamics study of ion selectivity and conductivity in the potassium channel, Chem. Phys. Lett. 313 (1999) 358–365.
[10] D. Chen, J. Lear, R.S. Eisenberg, Permeation through an open channel: Poisson–Nernst–Planck theory of a synthetic ionic channel, Biophys. J. 72 (1997) 97–116.
[11] D. Chen, L. Xu, A. Tripathy, G. Meissner, B. Eisenberg, Permeation through the calcium release channel of cardiac muscle, Biophys. J. 73 (1997) 1337–1354.
[12] W. Nonner, D. Chen, B. Eisenberg, Anomalous mole fraction effect, electrostatics, and binding in ionic channels, Biophys. J. 74 (1998) 2327–2334.
[13] W. Nonner, R.S. Eisenberg, Ion permeation and glutamate residues linked by Poisson–Nernst–Planck theory in L-type calcium channels, Biophys. J. 75 (1998) 1287–1305.
[14] D.P. Chen, L. Xu, A. Tripathy, G. Meissner, B. Eisenberg, Selectivity and permeation in calcium release channel of cardiac muscle: alkali metal ions, Biophys. J. 76 (1999) 1346–1366.
[15] M.G. Kurnikova, R.D. Coalson, P. Graf, A. Nitzan, A lattice relaxation algorithm for three-dimensional Poisson–Nernst–Planck theory with application to ion transport through the gramicidin A channel, Biophys. J. 76 (1999) 642–656.
[16] R.S. Eisenberg, Computing the field in proteins and channels, J. Membr. Biol. 150 (1996) 1–25.
[17] R.S. Eisenberg, From structure to function in open ionic channels, J. Membr. Biol. 171 (1999) 1–24.
[18] B. Corry, S. Kuyucak, S.H. Chung, Test of Poisson–Nernst–Planck theory in ion channels, J. Gen. Physiol. 114 (1999) 597–599.
[19] B. Corry, S. Kuyucak, S.H. Chung, Tests of continuum theories as models of ion channels: II. Poisson–Nernst–Planck theory versus Brownian dynamics, Biophys. J. 78 (2000) in press.
[20] R.M. Lynden-Bell, J.C. Rasaiah, Mobility and solvation of ions in channels, J. Chem. Phys. 105 (1996) 9266–9280.
[21] T.W. Allen, S. Kuyucak, S.H. Chung, The effect of hydrophobic and hydrophilic channel walls on the structure and diffusion of water and ions, J. Chem. Phys. 111 (1999) 7985–7999.
[22] G.R. Smith, M.S.P. Sansom, Dynamic properties of Na^+ ions in models of ion channels: a molecular dynamics study, Biophys. J. 75 (1998) 2767–2782.
[23] G.R. Smith, M.S.P. Sansom, Effective diffusion coefficients of K^+ and Cl^- ions in ion channel models, Biophys. Chem. 79 (1999) 129–151.
[24] T.W. Allen, A. Bliznyuk, A.P. Rendell, S. Kuyucak, S.H. Chung, The potassium channel: structure, selectivity and diffusion, J. Chem. Phys. 112 (2000) in press.
[25] E. Perozo, D.M. Cortes, L.G. Cuello, Structural rearrangements underlying K^+-channel activation gating, Science 285 (1999) 73–78.
[26] B.R. Brooks, R.E. Bruccoleri, B.D. Olafson, D.J. States, S. Swaminathan, M. Karplus, CHARMM: a program for macromolecular energy, minimization, and dynamics calculations, J. Comp. Chem. 4 (1983) 187–217.
[27] T. Lazaridis, M. Karplus, Effective energy function for proteins in solution, Proteins 35 (1999) 133–152.
[28] H.J.C. Berendsen, J.R. Grigera, T.P. Straatsma, The missing term in effective pair potentials, J. Phys. Chem. 91 (1987) 6269–6271.
[29] W.L. Jorgensen, J. Chandrasekhar, J.D. Madura, R.W. Impey, M.L. Klein, Comparison of simple potential

functions for simulation of liquid water, J. Chem. Phys. 79 (1983) 926–935.
[30] M.S.P. Sansom, I.D. Kerr, J. Breed, R. Sankararamakrishnan, Water in channel-like cavities: structure and dynamics, Biophys. J. 70 (1996) 693–702.
[31] B.M. Pettit, P.J. Rossky, Alkali halides in water: ion-solvent correlations and ion–ion potentials of mean force at infinite dilution, J. Chem. Phys. 84 (1986) 5836–5844.
[32] E. Guàrdia, J.A. Padró, Molecular dynamics simulation of single ions in aqueous solutions: effects of the flexibility of the water molecules, J. Phys. Chem. 94 (1990) 6049–6055.
[33] K. Heinzinger, Computer simulations of aqueous electrolyte solutions, Physica B 131 (1985) 196–216.
[34] G.S. DelBuono, T.S. Cohen, P.J. Rossky, Effects of long-range interactions on the dynamics of ions in aqueous solutions, J. Mol. Liquids 60 (1994) 221–236.
[35] L. Perera, U. Essmann, M.L. Berkowitz, Effect of the treatment of long-range forces on the dynamics of ions in aqueous solutions, J. Chem. Phys. 102 (1995) 450–456.
[36] T.W. Allen, S. Kuyucak, S.H. Chung, Molecular dynamics study of the KcsA potassium channel, Biophys. J. 77 (1999) 2502–2516.
[37] D.C. Rapaport, The Art of Molecular Dynamics Simulation, Cambridge University Press, Cambridge, 1995.
[38] D.R. Lide, (Ed.), CRC Handbook of Chemistry and Physics CRC Press, Cleveland, 1994.
[39] D. Eisenberg, W. Kauzmann, The Structure and Properties of Water, Oxford University Press, London, 1969.
[40] N.T. Skipper, G.W. Neilson, X-ray and neutron diffraction studies on concentrated aqueous solutions of sodium nitrate and silver nitrate, J. Phys. Cond. Matt. 1 (1989) 4141–4154.
[41] G.W. Neilson, N.T. Skipper, K^+ coordination in aqueous solution, Chem. Phys. Lett. 114 (1985) 35–38.
[42] N.A. Hewish, G.W. Neilson, J.E. Enderby, Environment of Ca^{2+} ions in aqueous solvent, Nature 297 (1982) 138–142.
[43] A.K. Soper, G.W. Neilson, J.E. Enderby, R.A. Howe, A neutron diffraction study of hydration effects in aqueous solutions, J. Phys. C10 (1977) 1793–1801.
[44] S. Obst, H. Bradaczek, Molecular dynamics study of the structure and dynamics of the hydration shell of alkaline and alkaline-earth metal cations, J. Phys. Chem. 100 (1996) 15677–15687.
[45] B. Roux, M. Karplus, Ion transport in a gramicidin-like channel: dynamics and mobility, J. Phys. Chem. 95 (1991) 4856–4868.